

Freezing Behavior of Single Sulfuric Acid Aerosols Suspended in a Quadrupole Trap

K.L. Carleton, D.M. Sonnenfroh, W.T. Rawlins, B.E. Wyslouzil, and S. Arnold

Journal of Geophysical Research **102**, 6025, (1997).

Copyright 1997 by the American Geophysical Union. Permission is granted to use short quotes, figures, and tables for publication in scientific books and journals or for distribution to students for classroom use. For permission for any other use, contact the AGU Publications Office at AGU, 200 Florida Ave., N.W., Washington, D.C. 20009. Further electronic distribution is not allowed.

0305 Aerosols and Particles
FREEZING BEHAVIOR OF SINGLE SULFURIC ACID AEROSOLS
SUSPENDED IN A QUADRUPOLE TRAP

K.L. Carleton, D.M. Sonnenfroh, W.T. Rawlins
(Physical Sciences Inc., 20 New England Business
Center, Andover, MA 01810)

B.E. Wyslouzil, S. Arnold

The freezing properties of sulfuric acid droplets were studied by suspending single 20 to 30 μm diameter particles in a quadrupole trap and cooling them to stratospheric temperatures (≥ 191.5 K). Each particle's DC balance voltage was measured to determine the particle composition as a function of temperature and map out the particle's trajectory relative to the sulfuric acid phase diagram. Angularly resolved optical scattering patterns were monitored to detect freezing events. Particles cooled through the sulfuric acid tetrahydrate region (35 to 70 wt% H_2SO_4) did not freeze, and remained spherical liquid droplets for several hours. Only particles cooled through the ice-liquid equilibrium region (< 35 wt% H_2SO_4) showed evidence of freezing. This supports previous experimental and field observations that stratospheric sulfuric acid aerosols are likely to remain liquid to within a few degrees of the ice frost point. (Aerosols, sulfuric acid, phase transition, polar stratospheric cloud.)

0320, 0340, 0365

FREEZING BEHAVIOR OF SINGLE SULFURIC ACID AEROSOLS SUSPENDED IN A QUADRUPOLE TRAP

K.L. Carleton, D.M. Sonnenfroh, W.T. Rawlins
Physical Sciences Inc.
20 New England Business Center
Andover, MA 01810

B.E. Wyslouzil
Department of Chemical Engineering
Worcester Polytechnic Institute
100 Institute Rd.
Worcester, MA 01609-2280

S. Arnold
Microparticle Photophysics Labs (MP³L)
Polytechnic University
6 Metrotech Center
Brooklyn, NY 11201

ABSTRACT

The freezing properties of sulfuric acid droplets were studied by suspending single 20 to 30 μm diameter particles in a quadrupole trap and cooling them to stratospheric temperatures (≥ 191.5 K). Each particle's DC balance voltage was measured to determine the particle composition as a function of temperature and map out the particle's trajectory relative to the sulfuric acid phase diagram. Angularly resolved optical scattering patterns were monitored to detect freezing events. Particles cooled through the sulfuric acid tetrahydrate region (35 to 70 wt% H_2SO_4) did not freeze, and remained spherical liquid droplets for several hours. Only particles cooled through the ice-liquid equilibrium region (< 35 wt% H_2SO_4) showed evidence of freezing. This supports previous experimental and field observations that stratospheric sulfuric acid aerosols are likely to remain liquid to within a few degrees of the ice frost point.

INTRODUCTION

Polar stratospheric clouds (PSCs) are composed of solid nitric acid hydrates, primarily nitric acid trihydrate (NAT) [Crutzen and Arnold, 1986; Toon *et al.*, 1986; Solomon, 1990]. These solid particles are thought to nucleate on the background sulfuric acid aerosols at temperatures below ≈ 195 K. However, the mechanism for this process is uncertain. It has been proposed that the sulfuric acid aerosols need to freeze in order to efficiently nucleate the NAT phase [Poole and McCormick, 1988; Tolbert, 1994a]. Since typical stratospheric compositions of sulfuric acid are in the 40-70 wt% range, the most likely sulfuric acid hydrate phase which would form upon freezing is sulfuric acid tetrahydrate (SAT) [Gable *et al.*, 1950].

A variety of theoretical calculations, field measurements and laboratory studies have been performed to determine the most likely phase of the background sulfuric acid aerosols under conditions important in the stratosphere. Several investigators have used classical nucleation theory to calculate the fate of sulfuric acid aerosols. Preliminary calculations suggested that freezing of a large fraction (50%) of the aerosol could occur over time scales of a few hours at 195-205 K for 60 wt% solutions [Luo *et al.*, 1992]. However, more recent calculations yielded insignificant freezing rates ($<10^{-3}$ cm³ s⁻¹) for supercooled H₂SO₄ droplets under similar conditions [Luo *et al.*, 1994]. Other results suggest that freezing may occur within a few degrees of the ice frost point [Jensen and Toon, 1991]. The disparity of these results arises from the sensitivity of these calculations to input parameters, especially the surface tension of the ice-liquid interface, σ_{il} . Uncertainties of a factor of 2 in σ_{il} can yield nucleation rates which differ by more than 10 orders of magnitude [Luo *et al.*, 1994; Larsen, 1994].

Field measurements of the particle size distribution during the Airborne Arctic Stratosphere Experiment were examined for evidence of sulfate aerosol freezing. Dye *et al.* [1992] examined

the evolving size distribution as the air temperature decreased. They observed deliquescence of the sulfate aerosols which followed the behavior expected for liquid droplets, suggesting that these aerosols remained liquid down to at least 193 K. These temperatures are lower than those at which NAT was observed. Therefore, freezing of sulfuric acid aerosols did not appear to be a key step in the formation of PSCs during these Arctic flights.

Several laboratory studies of the freezing properties of bulk sulfuric acid samples have indicated that sulfuric acid can efficiently supercool under stratospheric conditions [*Ohtake, 1993; Zhang et al., 1993a; Middlebrook et al., 1993*]. Visual observations of bulk solutions yielded freezing temperatures of less than 200 K in the SAT region [*Ohtake, 1993*]. FTIR observations of sulfuric acid hydrate formation in thin films exhibited colder freezing temperatures, as low as 1 to 4 K below the ice frost point [*Middlebrook et al., 1993*]. Recent data show that ternary solutions of sulfuric acid, nitric acid and water can easily form, with nitric acid solubilities increasing strongly for more dilute sulfuric acid solutions [*Zhang et al., 1993b; Molina et al., 1993*]. This suggests that NAT may actually nucleate from the ternary liquid droplets to produce PSC cloud particles. Indeed, nucleation of NAT films has been observed at moderate nitric acid supersaturations over liquid sulfuric acid films, with consequent freezing of the sulfuric acid, while extremely high supersaturations of nitric acid were required to nucleate NAT on frozen sulfuric acid films [*Iraci et al., 1994; Tolbert, 1994b*]. In contrast, *Koop et al. [1995]* found premixed ternary bulk solutions to be resistant to freezing at temperatures as low as 185 K. Experiments utilizing sub-micron binary sulfuric acid/water aerosols entrained in low temperature flow tubes or cells observed no freezing for compositions in any region of the phase diagram outside the ice equilibrium region for temperatures as low as 189 K [*Miller, 1995; Sloan, 1995; Anthony et al., 1995*].

The investigations reported here were performed to complement previous bulk and aerosol freezing studies by examining the freezing behavior of single sulfuric acid droplets held at stratospheric temperatures for several hours. Single liquid aerosols of 20 to 30 μm diameter were electrically suspended in an electrodynamic levitator so that they did not contact any surfaces. This wall-less confinement removes any complications from heterogeneous nucleation. Freezing behavior was examined at temperatures down to 191.5 K for varying gas phase relative humidity to study freezing probabilities as a function of particle composition.

EXPERIMENTAL METHODS

Single aerosol particles are suspended in an electrodynamic levitator or trap which is contained in an environmentally controlled chamber [Wyslouzil *et al.*, 1994]. The electrodynamic trap is similar in concept to a Millikan oil drop apparatus and can be used to suspend charged particles for extensive periods of time (few hours to days). Our spherical void electrodynamic levitator is composed of three cylindrical electrodes with a central void which is spherical in shape (Figure 1a) [Arnold and Folan, 1987]. This geometry works similarly to the more conventional hyperbolic design [Paul, 1990; Wuerker *et al.*, 1959]. The central ring electrode is biased with an AC voltage (100 to 1000 V_{rms}, 60 Hz) which creates the trapping potential. The endcaps are biased with a DC voltage (0 to 100 V) which offsets the gravitational force on the particle. A snapshot of the calculated electric field in the trap shows the saddle potential which alternately confines the particle in the axial and radial directions as the AC field varies (Figure 1b).

The DC balancing voltage is related to the particle mass by:

$$V_{dc} = mgz_0 / qC \quad (1)$$

where V_{dc} is the applied DC field, m and q are the particle's mass and charge, g is the gravitational acceleration, z_0 is one half the trap's end cap spacing, and C is a geometric constant (equal to ≈ 0.45 for the spherical void trap geometry used in these experiments). For a fixed particle charge, the particle mass is directly related to the DC voltage and can be measured [Philip *et al.*, 1983; Arnold, 1979]. Changes in the balance voltage can then be used to determine relative changes in particle mass. The extremely low vapor pressure of sulfuric acid ensures that any change in mass is the result of exchange of water with the gas phase. Therefore, the balance voltage is directly related to the particle composition. This assumes that the particle charge remains constant, as verified by observations of constant particle charge over time scales of several days. The DC voltage required to balance the particle is determined by viewing the particle's image with a microscope based camera system (see below) and adjusting the DC voltage to center the particle in the trap. The voltage is measured with a digital voltmeter. Measured voltages are reproducible to ± 0.5 V (for 30 to 40 V balancing voltages) which corresponds to errors in relative mass of less than 2%.

In order to simulate stratospheric conditions, the trap is enclosed in a double-jacketed, temperature controlled chamber. The inner chamber is made of copper and is mounted on a cooled block to provide a uniform temperature environment. The outer chamber remains at room temperature. The space between the two chambers is evacuated to $< 10^{-4}$ torr with a two stage roughing pump to minimize thermal loads. Each chamber has windows to provide the necessary optical access. Approximately 10 W of cooling is provided to the cold block by a copper rod which is connected to a liquid nitrogen cold finger outside of the chamber. The heat transfer rate

is proportional to the temperature difference between the trap and the cold finger. As a result, cooling rates vary from 20 K hr⁻¹ when the trap is at room temperature to 1 to 2 K hr⁻¹ at 191 K, which can be reached with 12 hours of cooling.

Temperatures are measured with several different thermocouples which have been calibrated to a NIST traceable standard to an accuracy of 0.1 °C. In addition, gas temperatures were measured with a thermocouple suspended above the trap while gas was flowed through the system at our typical operating flow rate (100 sccm). Gas temperatures measured in this way were higher than wall temperatures by 1.5 °C or less. Simple thermal analysis shows that this discrepancy is the result of conductive loads on the suspended thermocouple from its room temperature mounting and not convective gas loads from the slow gas flow rates used here. All temperatures quoted in this work are those measured by the mechanically mounted thermocouple attached to the top of the trap stand.

The gas phase relative humidity in the trap is controlled with a saturator system in which dry nitrogen diluent is combined with nitrogen flowed through the water saturator. The humidity is varied from 0 to 100% at room temperature by adjusting the relative flow rates of the two streams. An optional liquid nitrogen trap permits further dehydration of the gas stream. The total gas flow rate is held fixed at 100 sccm. This flow rate gives a reasonable cell equilibration time without inducing aerodynamic drag on the particle sufficient to perturb the particle balancing voltage. The water activity or relative humidity (RH) in the trap is related to the flow rates and the temperatures in the system by:

$$\text{RH} = \frac{F_{\text{sat}} P_{\text{sat}}(T_{\text{sat}})}{((F_{\text{sat}} + F_{\text{bypass}}) P_{\text{trap}}(T_{\text{trap}}))} \quad (2)$$

where F_{sat} is the flow rate of nitrogen through the water saturator, F_{bypass} is the bypass dry nitrogen flow rate, $P_{\text{sat}}(T_{\text{sat}})$ is the vapor pressure of water at the saturator temperature, and $P_{\text{trap}}(T_{\text{trap}})$ is the vapor pressure of water at the trap temperature. This method assumes equilibrium between the liquid and vapor phases in the saturator at the saturator temperature. The method was verified by measuring the dew point of the mixed stream using an EG&G model 911 digital humidity analyzer. The two determinations agree to within 3 to 5%. Two calibrated T-type thermocouples are used to measure T_{sat} and T_{trap} .

Particles suspended in the trap are probed with optical diagnostics as shown in Figure 2. Optical scattering is used to view the particle and to size it by measuring its angular scattering pattern. The particle is illuminated with a 3 mW, linearly polarized HeNe laser beam which passes through an aperture in the ring electrode. The light scattered from the particle at 90 deg (relative to the initial laser beam direction) is imaged with a microscope based camera system and is viewed on a small monitor.

The HeNe scattered light is also detected through a slit in the ring electrode by the linear array of an Optical Multichannel Analyzer (OMA) system to obtain angularly resolved Mie scattering patterns. The OMA has an intensifier with 700 pixels on 25 μm centers. It is located 10.5 cm from the particle at either 45 or 90 deg from the forward scattering direction. Angular scattering is observed in the forward quadrant over a 10 deg spread with a resolution of approximately 0.02 deg per pixel. Time-averaged angular scattering distributions were recorded every 1 s.

During the course of cooling a single sulfuric acid particle, its composition must be monitored to determine what part of the phase diagram is being sampled. Composition is determined by comparing the relative balance voltage with that measured for the initial

conditions. The initial particle composition is determined from the thermodynamic relationships between composition and gas phase relative humidity [Zeleznik, 1991] at room temperature for several initial relative humidities (typically 10, 20, 30 and 50% RH). These results are analyzed by a fitting procedure to yield the amount of sulfuric acid present in the drop. From this fit, we obtain a balance voltage, V_i , for a reference relative humidity. Any subsequent change in particle composition, W (wt%) is related to the initial reference composition, W_i and balance voltage by the new balance voltage, V :

$$W = W_i V_i/V \quad (3)$$

The particle composition can therefore be measured without further need to monitor the gas phase composition. Uncertainties in the initial humidity fits ($\pm 5\%$ of V_{dc}) and the relative humidity produced from the saturator ($\pm 3\%$ RH) result in uncertainties in the final particle composition ranging from ± 2 wt% for dilute drops (30 to 40 wt%) to ± 4 wt% for higher concentration drops (60 to 70 wt%).

Particles studied in this work were 20 to 30 μm diameter sulfuric acid droplets suspended in the quadrupole trap. The droplets are injected using a microparticle on-demand picopipette [Arnold and Folan, 1986]. As the particle is cooled down, a slow flow of nitrogen (100 sccm) is passed through the quadrupole trap chamber. As described above, the amount of water in the gas phase in the quadrupole trap can be varied by adjusting the combination of the saturator and diluent flow rates, or by drying the gas cryogenically. These methods allow us to control the "trajectory" of the particle across the phase diagram.

Particle phase is monitored by angularly-resolved optical scattering. Spherical (liquid) droplets have periodic angular Mie scattering patterns, while nonspherical (solid) particles have

more complex scattering patterns. Therefore, a stable, periodic Mie pattern is evidence of a spherical and hence a liquid droplet. As discussed below, we have observed frozen sulfuric acid particles which exhibit a loss of this periodic Mie pattern. There may be situations in which an initially liquid particle might remain spherical following a freezing event, particularly with sulfuric acid which becomes highly viscous at stratospheric temperatures [Williams and Long, 1995]. We therefore monitor other data in addition. Because the heat of fusion is released as the particle changes phase, there is a temperature change which manifests itself as a change in balance voltage as the particle's H₂O content responds. We continuously monitor the balance voltage during the experiments.

RESULTS

Several different particles were cooled to examine different final compositions for evidence of phase changes and to demonstrate reproducibility. The particle cooling trajectories sampled the ice-liquid and sulfuric acid hemihexahydrate (SAH), tetrahydrate (SAT), dihydrate (SAD), and monohydrate (SAM) regions of the equilibrium phase diagram of H₂SO₄/H₂O. A summary of the observed endpoints is given in Table 1. In all seven cases of particles cooled to sulfuric acid hydrate compositions (>37 wt% H₂SO₄), no evidence of freezing was observed. A typical particle cooling trajectory is shown in Figure 3, superimposed on the sulfuric acid phase diagram [Gable *et al.*, 1950]. This trajectory was achieved by drying the nitrogen gas as much as possible and as soon as possible after cooling began. The final drop temperature was 191.5 K at 61 wt% H₂SO₄.

Angular scattering patterns for the initial room temperature droplet and the final cold particle of Figure 3 are shown in Figure 4. After several hours below 192 K, the scattering

pattern was still periodic and essentially unchanged from that of the initial room temperature liquid, signifying that the droplet was still spherical and liquid. This corresponds to supercooling of 52 K without freezing. Similar results were observed for six other particles cooled through the sulfuric acid hydrate regions of the phase diagram.

Two particles were cooled into the ice-liquid equilibrium region (<36 wt% H_2SO_4) in order to observe and confirm the effects of freezing on the angular scattering distribution and mass uptake response. Only one particle was clearly observed to freeze. This trajectory is shown as the dashed curve in Figure 5. The particle was cooled through the ice-liquid equilibrium region by maximizing the amount of water in the quadrupole trap during cooling. As soon as the particle trajectory crossed the ice-liquid equilibrium line, the angular scattering distribution began to vary as illustrated in Figure 6. The distribution fluctuated between a single, Mie-type periodic pattern (Figure 6b) and a beat pattern which had the same period but had a second beat frequency superimposed on the primary peak intensities (Figure 6a). As the particle continued to cool, the scattering pattern eventually changed to a persistent, non-periodic distribution (Figure 6c) characteristic of an irregularly shaped particle. The compositions and temperatures at which the transitory, periodic (just prior to freezing), and non-periodic scattering patterns were observed are shown on the trajectory of Figure 5 as points 1a, 1b and 1c, respectively.

It is difficult to determine conclusively the cause of the fluctuating scattering pattern (Figure 6a and 6b). The fluctuations between pattern a and pattern b suggest a transitory phenomenon preceding or related to the dynamics of the phase change. We have performed optical scattering calculations for several scenarios which produce scattering patterns similar to those we observed. The calculations suggest that the fluctuating pattern could be the result of going through a Mie resonance due to a change in index of refraction which might result from a

phase change, a radial gradient in the particle composition and hence index of refraction, or a slightly aspherical particle shape. Alternatively, it is also possible that the particle is compositionally inhomogeneous as would result if one or more ice crystals nucleated inside the liquid particle. In this case, motion of the crystals inside the liquid particle would produce random temporal fluctuations in the scattering pattern similar to those observed here [Bronk, et al., 1993]. In any event, it appears that the observed fluctuations are indicative of mixed-phase compositional changes just prior to freezing.

When the particle temperature approached the solid-solid tie line for ice and SAT, the particle suddenly froze, as indicated by the onset of a persistent, polymorphous angular scattering distribution (Figure 6c). The phase change is evidenced by the loss of periodicity in the scattering pattern. Simultaneously with this change in the scattering pattern's periodicity, the particle mass also changed suddenly, increasing by 6%. This mass increase is consistent with the conclusion of the freezing event and the completion of the release of the heat of fusion. As the gas phase continues to cool, the ongoing release of the heat of fusion causes the particle to remain at constant temperature during freezing. Once the particle is completely frozen and the heat release ends, the particle temperature quickly equilibrates with the colder temperature of the gas phase. The colder, frozen particle is then able to grow, acquiring mass through uptake of water.

It is interesting to consider the compositional changes in a mixed-phase particle during the freezing process. The optical scattering results suggest that the particle does not freeze instantaneously, but rather remains a dynamic mixture of ice and liquid until it finally freezes throughout at 202 K. If ice (0 wt% H₂SO₄) were nucleating in the interior of the droplet as the particle cooled, the liquid composition would become more concentrated, following the ice-

liquid equilibrium line in Figure 5. The lever rule can be used to estimate the partitioning of the particle between the ice and liquid phase. By drawing a horizontal line at the temperature of the particle, the lengths of the lines to the ice and liquid equilibrium lines are inversely proportional to the amount of each phase present. For example, at 207 K (point 1b) the average particle composition is 33 wt% H_2SO_4 . The length of the line to ice (0 wt%) is 11 times the length to the liquid equilibrium composition (36 wt%) so the particle would be 8% ice and 92% liquid. Under these conditions, the liquid composition would be enriched to 36 wt% H_2SO_4 , which is the composition of the liquid equilibrium line.

An additional particle was also cooled through the ice-liquid equilibrium region. It behaved somewhat differently from the previous particle in that its scattering pattern remained quasiperiodic, indicating it remained mostly liquid into the ice-liquid region. Its scattering pattern became temporally unstable at 206 K and 33.1 wt% H_2SO_4 . As with the previous particle, this instability consisted of the transitory addition of a second period superimposed on the primary periodicity. In addition, we also observed these multiperiodic scattering patterns when quickly dehydrating the particle. Examples of these scattering patterns are shown in Figure 7 with their locations indicated on the trajectory shown by the solid curve in Figure 5. After the scattering pattern became multiperiodic, the particle continued to cool and ended at 34.3 wt% and 192 K without losing the periodicity in its scattering pattern. The angular scattering patterns continued to fluctuate between the normal and multiperiodic distributions, however no complex patterns like Figure 6c occurred. This suggests that the particle did not become nonspherical and hence did not freeze completely. Furthermore, no sudden mass uptake signifying completion of the release of the heat of fusion occurred. The apparently dissimilar phase transition behavior exhibited by the two ice-liquid particles may be symptomatic of the

stochastic nature of the freezing process as described below. However, we note that the final average composition of the unfrozen particle is within experimental uncertainty of that of the hemihexahydrate phase, and transitory nucleation of ice crystals within the particle would push the composition of the remaining liquid toward higher H_2SO_4 concentrations where freezing clearly does not occur.

A summary of the minimum temperatures for all the particles studied is given in Table 1. Particles were held at these temperatures for one-half to two hours. However, because of the slow cooling rates of these experiments, in several cases the particles were within 1 K of the final temperature for at least the last hour of each run. The final endpoints are shown graphically in Figure 8 relative to the $\text{H}_2\text{SO}_4/\text{H}_2\text{O}$ phase diagram. Superimposed on Figure 8 are the equilibrium compositions for sulfuric acid particles for two fixed water partial pressures characteristic of the stratosphere (1×10^{-4} torr and 4×10^{-4} torr). The droplets that we monitored remained liquid at stratospheric compositions and well below the temperatures that one would normally encounter in the stratosphere.

DISCUSSION

Classical nucleation theory is often used to describe the freezing probabilities of aerosols. This theory assumes that germ nuclei must form and reach sufficiently large sizes to be stable. Once the embryos reach this critical size, they then grow via diffusion of liquid molecules to the nuclei, eventually causing the aerosol particle to freeze. The freezing process can therefore be separated into two processes: the formation of these critical nuclei and their subsequent growth. Either of these steps can limit the freezing probability of an aerosol particle.

It has recently been suggested that the high viscosity of cold sulfuric acid aerosols may limit molecular diffusion rates and hence the growth of these critical nuclei [Tabazadeh *et al.*, 1995]. Using the viscosity data from Williams and Long [1995], we can estimate diffusion coefficients and then diffusion times across a 1 μm diameter aerosol particle. The diffusion coefficient is related to viscosity by:

$$D = A T / \eta$$

where A is a constant, T is temperature in K, and η is the viscosity. Estimates of A for HCl in H_2SO_4 are $(0.2 \text{ to } 1) \times 10^{-7} \text{ cm}^2\text{cP K}^{-1}\text{s}^{-1}$ [Williams and Long, 1995]. Since H_2SO_4 will have a larger molecular diameter and A is inversely proportional to the molecular diameter ($A \approx k/l$ where l is the molecular diameter and k is Boltzmann's constant), let us assume a value of $10^{-8} \text{ cm}^2\text{cP K}^{-1}\text{s}^{-1}$ as a conservative lower bound. This, in conjunction with the measured H_2SO_4 viscosities, yields lower-bound diffusion coefficients at 190 K which range from $2.5 \times 10^{-10} \text{ cm}^2 \text{ s}^{-1}$ for 30 wt% H_2SO_4 to $2.6 \times 10^{-11} \text{ cm}^2 \text{ s}^{-1}$ for 65 wt% H_2SO_4 . For a diffusion distance of 1 μm , these values yield upper-bound diffusion times of 40 to 400 s. At 190 K, the aerosols are typically more dilute (≈ 40 wt% H_2SO_4) so that the shorter times should be the most relevant. Furthermore, a diffusion distance of 1 μm , used here as a guide, is extreme for the particles used in our experiments, and is obviously too large for the submicron atmospheric aerosols. Thus the diffusion rates are not constraining on the time scale of our experiments, nor are they slow enough to limit the freezing probabilities of atmospheric aerosols on the time scales of their exposure to low temperatures. Therefore, it is unlikely that the growth of the nuclei is impeded.

Since the freezing process should not be limited by the growth of the critical nuclei, it must be the formation of these nuclei which is the limiting step. Classical nucleation theory

relates the freezing probability of a droplet, $p(t)$, to the barrier for formation of these nuclei through the nucleation rate [Luo *et al.*, 1992; Pruppacher and Klett, 1978]:

$$p(t) = 1 - \exp[-J(T,\chi) V t] \quad (4)$$

where $J(T,\chi)$ is the nucleation rate as a function of temperature T and composition χ , V is the droplet volume, and t is the time. In this simple formalism, the freezing probability is proportional to particle volume. In our experimental studies, 20 to 30 μm (diameter) particles were used. Because droplet volume and time at temperature are both involved in calculating the freezing probability, we can extrapolate our short term observations of 20 μm particles to long term behavior of the submicron stratospheric aerosol layer. Observing 20 μm particles for 1 hour at low temperatures is equivalent to observing 1 μm particles for 8000 hours or approximately 1 year. This is comparable to the natural lifetime of the background sulfate aerosol. Since we do not see evidence for freezing in the sulfuric acid tetrahydrate (SAT) part of the phase diagram for the large particles, the laboratory measurements imply that the background stratospheric aerosol is predominantly liquid at temperatures above 191 K.

In the limit of classical nucleation theory, we can use the current results to estimate an upper bound for the embryo nucleation rate. Rearranging Eq. (4) and solving for J gives:

$$J = -\ln(1-p)/V t \quad (5)$$

In the present experiments, no particles in the SAT region were observed to freeze. If we assume that the probability of freezing is less than 5% (2σ confidence limit), we can solve for upper bounds for J based on drop volumes and observation times as shown in Table 2. Here, observation times are taken as the amount of time that the drop was within 1 K of the final

droplet temperature. The lowest upper bound for J is $310 \text{ cm}^{-3} \text{ s}^{-1}$, which is 5 to 10 orders of magnitude larger than values predicted by theoretical calculations (5×10^{-8} to $5 \times 10^{-4} \text{ cm}^{-3} \text{ s}^{-1}$) [Luo *et al.*, 1992, 1994]. However, the experimental upper bound for J still predicts less than 0.004% probability for particles of $0.1 \text{ }\mu\text{m}$ radius to freeze after 1 year at a temperature of 191 K (or 4% for $1 \text{ }\mu\text{m}$ radius). Most particles do not spend this long a time period at the coldest temperatures. Therefore, extrapolation of our laboratory results within the context of this theory indicates that stratospheric $\text{H}_2\text{SO}_4/\text{H}_2\text{O}$ aerosols are unlikely to be frozen.

These results are consistent with other laboratory observations that sulfuric acid aerosols are unlikely to freeze at typical stratospheric temperatures ($>190 \text{ K}$) and compositions ($>35 \text{ wt}\%$ H_2SO_4). Bulk samples (10 ml) held in test tubes were observed to supercool and then freeze at temperatures of 200-205 K [Ohtake, 1993]. However, freezing typically nucleated at the tip of an immersed thermocouple and is therefore most likely heterogeneous [Luo *et al.*, 1994]. Other bulk freezing studies of varying sample size ($5 \text{ }\mu\text{l}$ - 3 ml) showed no evidence of freezing after 24 hours at 203 to 230 K [Molina *et al.*, 1993]. Additional studies of bulk solutions by Beyer *et al.* [1994] showed freezing after supercooling in the ice-liquid region, consistent with that reported here, and extremely low freezing probabilities after many hours of exposure at 180 to 200 K in the SAT regime. Interestingly, Beyer *et al.* [1994] also observed glass formation upon cooling $>36 \text{ wt}\%$ H_2SO_4 solutions to $\approx 150 \text{ K}$, followed by freezing upon warming to 180 to 190 K. This observation is consistent with diffusion-limited freezing near 150 K and nucleation-limited freezing above 180 K, in agreement with our analysis above.

Thin H_2SO_4 films of a few μm thickness showed varying freezing behavior with some films freezing at 195-200 K, but many did not freeze until temperatures were below the ice frost point [Middlebrook *et al.*, 1993]. The investigators suggested that SAT may have nucleated on the

silicon support and the events which did lead to frozen films were the result of heterogeneous phase transitions. Several aerosol flow tube experiments have made observations of small aerosols (0.1 to 0.2 μm) for short times (30 s [Miller, 1995; Sloan, 1995] to 1 to 2 hours [Anthony *et al.*, 1995]). These experiments also only observe freezing in the ice-liquid equilibrium regions at the coldest temperatures. Our results also support field observations that suggest that stratospheric aerosols are liquid down to temperatures as low as 193 K [Dye *et al.*, 1992].

Our preliminary results for more dilute droplet compositions (<35 wt% H_2SO_4) show that freezing is more likely if droplets cool through the ice-liquid equilibrium region. To achieve compositions in this region requires much greater water vapor mixing ratios than the normal stratospheric levels. While these conditions are unlikely in the stratosphere, they may be encountered in aircraft exhaust plumes or tropopause folding events. They may also occur during the formation of cirrus ice clouds. Freezing may also be enhanced by heterogeneous nucleation on undissolved materials such as dust or soot [Luo *et al.*, 1994]. We have recently demonstrated [Wyslouzil *et al.*, 1994] that deposition of H_2SO_4 on carbon particles activates them as CCN, raising the possibility that a significant fraction of $\text{H}_2\text{SO}_4/\text{H}_2\text{O}$ aerosols in the atmosphere may contain a solid core. We are continuing to investigate phase change behavior relevant to multicomponent aerosols including aqueous sulfuric acid aerosols seeded with carbon.

In the non-volcanic lower stratosphere, it is unlikely that binary sulfuric acid particles can exist below temperatures of about 194 K, owing to the propensity for rapid HNO_3 uptake at lower temperatures [Molina *et al.*, 1993; Tabazadeh *et al.*, 1994; Carslaw *et al.*, 1994, 1995]. Below 192 K, the stratospheric particles become mostly $\text{HNO}_3/\text{H}_2\text{O}$, with small mass fractions of H_2SO_4 [Tabazadeh *et al.*, 1994], and NAT may nucleate out of the solution or on the particle surfaces [Iraci *et al.*, 1994; Beyer *et al.*, 1994]. In addition, thermal cycling of the particles may

trigger NAT or SAT nucleation [Tabazadeh *et al.*, 1994; Iraci *et al.*, 1994]. We are investigating these issues in studies of the freezing dynamics of ternary single droplets using Raman spectroscopy to monitor composition and phase.

CONCLUSIONS

We have held single 20 to 30 μm (diameter) sulfuric acid droplets at temperatures of 191 to 200 K for periods of several hours and have observed no phase transition for particles cooled through the sulfuric acid tetrahydrate (SAT) equilibrium region. These particles had compositions typical of aerosols in the stratosphere (40 to 70 wt% H_2SO_4), and were cooled to lower temperatures than typically encountered for the comparable stratospheric compositions. These large particles would be more likely to freeze during our measurement time than the 0.1 to 1 μm particles typically found in the stratosphere. Therefore, these results imply that stratospheric sulfuric acid aerosols are most likely liquid prior to HNO_3 uptake. This supports current theories of polar stratospheric cloud nucleation which require dissolution of HNO_3 in supercooled, liquid sulfuric acid droplets. The only particle which was experimentally observed to freeze was one which cooled through the ice-liquid equilibrium region of the phase diagram. Therefore, the detailed temperature and composition histories of cloud particles are important in determining whether a phase transition occurs.

The resistance of concentrated sulfuric acid particles to freezing appears to result from prohibitively slow rates of embryonic nuclei formation near and above 180 to 190 K. The reason for this slow nucleation rate remains to be identified; however we note that sulfuric acid solutions contain significantly higher concentrations of the HSO_4^- anion at higher ionic strengths [Clegg and Brimblecombe, 1995], which may hinder the formation of polyhydrate structures.

Additional stratospheric aerosol freezing mechanisms, including HNO₃ uptake, temperature cycling, and heterogeneous freezing induced by a solid core, need further investigation.

ACKNOWLEDGMENTS - This research was supported by the NASA Atmospheric Effects of Aviation Program.

REFERENCES

- Anthony, S.E., R.T. Tisdale, R.S. Disselkamp, M.A. Tolbert, and J.C. Wilson, FTIR studies of low temperature sulfuric acid aerosols, *Geophys. Res. Lett.*, 22, 1105-1108, 1995.
- Arnold, S. Determination of particle mass and charge by one electron differentials, *J. Aerosol. Sci.*, 10, 49-53, 1979.
- Arnold, S. and L.M. Folan, Fluorescence spectrometer for a single electrostatically levitated microparticle, *Rev. Sci. Instrum.*, 57, 2250-2253, 1986.
- Arnold, S. and L.M. Folan, Spherical void electrodynamic levitator, *Rev. Sci. Instrum.*, 58, 1732-1735, 1987.
- Beyer, K.D., S.W. Seago, H.Y. Chang, and M.J. Molina, Composition and freezing of aqueous H₂SO₄/HNO₃ solutions under polar stratospheric conditions, *Geophys. Res. Lett.*, 21, 871-874, 1994.
- Bronk, B.V., M.J. Smith, and S. Arnold, Photon correlation spectroscopy for small spherical inclusions in a micron-sized electrostatically levitated droplet, *Opt. Lett.*, 18, 93-95, 1993.

- Carslaw, K.S., S.L. Clegg, and P. Brimblecombe, A Thermodynamic model of the system HCl-HNO₃-H₂SO₄-H₂O, including solubilities of HBr, from <200 to 328 K, *J. Phys. Chem.*, *99*, 11557-11574, 1995.
- Carslaw, K.S., B.P. Luo, S.L. Clegg, T. Peter, P. Brimblecombe, and P. Crutzen, Stratospheric aerosol growth and HNO₃ gas phase depletion from coupled HNO₃ and water uptake by liquid particles, *Geophys. Res. Lett.*, *21*, 2479-2482, 1994.
- Clegg, S.L., and P. Brimblecombe, Application of a multicomponent thermodynamic model to activities and thermal properties of 0-40 mol kg⁻¹ aqueous sulfuric acid from <200 to 328 K, *J. Chem. Eng. Data*, *40*, 43-64, 1995.
- Crutzen, P.J. and F. Arnold, Nitric acid cloud formation in the cold Antarctic stratosphere: A major cause for the springtime ozone hole, *Nature*, *324*, 651-655, 1986.
- Dye, J.E., D. Baumgardner, B.W. Gandrud, S.R. Kawa, K.K. Kelly, M. Loewenstein, G.V. Ferry, K.R. Chan, and B.L. Gary, Particle size distributions in Arctic polar stratospheric clouds, growth and freezing of sulfuric acid droplets and implications for cloud formation, *J. Geophys. Res.*, *97*, 8015-8034, 1992.
- Gable, C.M., H.F. Betz, and S.H. Maron, Phase equilibria of the system sulfur trioxide-water, *J. Amer. Chem. Soc.*, *72*, 1445-1448, 1950.
- Iraci, L.T., A.M. Middlebrook, M.A. Wilson, and M.A. Tolbert, Growth of nitric acid hydrates on thin sulfuric acid films, *Geophys. Res. Lett.*, *21*, 867-870, 1994.
- Jensen, E.J. and O.B. Toon, Homogeneous freezing nucleation of stratospheric solution droplets, *Geophys. Res. Lett.*, *18*, 1857-1860, 1991.
- Koop, T., U.M. Biermann, W. Raber, B.P. Luo, P.J. Crutzen, and Th. Peter, Do stratospheric aerosol droplets freeze above the ice frost point?, *Geophys. Res. Lett.*, *22*, 917-920, 1995.

- Larsen, N., The impact of freezing of sulfate aerosols on the formation of polar stratospheric clouds, *Geophys. Res. Lett.*, *21*, 425-428, 1994.
- Luo, B., T. Peter, and P.J. Crutzen, Maximum supercooling of H₂SO₄ acid aerosol droplets, *Ber. Bunsenges. Phys. Chem.*, *96*, 334-338, 1992.
- Luo, B., T. Peter, and P. Crutzen, Freezing of stratospheric aerosol droplets, *Geophys. Res. Lett.*, *21*, 1447-1450, 1994.
- Middlebrook, A.M., L.T. Iraci, L.S. McNeill, B.G. Koehler, M.A. Wilson, O.W. Saastad, M.A. Tolbert and D.R. Hanson, Fourier transform - infrared studies of thin H₂SO₄/H₂O films: Formation, water uptake and solid-liquid phase changes, *J. Geophys. Res.*, *98*, 20473-20481, 1993.
- Miller, R. Refractive Index Data from Aerosol Spectroscopy, Application to Model Polar Stratospheric Clouds, American Chemical Society meeting, Chicago, August 1995.
- Molina, M.J., R. Zhang, P.J. Wooldridge, J.R. McMahon, J.E. Kim, H.Y. Chang, and K.D. Beyer, Physical chemistry of the H₂SO₄/HNO₃/H₂O System : Implications for polar stratospheric clouds, *Science*, *261*, 1418-1423, 1993.
- Ohtake, T., Freezing points of H₂SO₄ aqueous solutions and formation of stratospheric ice clouds, *Tellus*, *45B*, 138-144, 1993.
- Paul, W., Electromagnetic traps for charged and neutral particles, *Rev. Mod. Phys.*, *62*, 531-540, 1990.
- Philip, M.A., F. Gelbard, and S. Arnold, An absolute method for aerosol particle mass and charge measurement, *J. Coll. Int. Sci.*, *91*, 507-515, 1983.
- Poole, L.R., and M.P. McCormick, Polar stratospheric clouds and the Antarctic ozone hole, *J. Geophys. Res.* *93*, 8423-8430, 1988.

- Pruppacher, H.R., and J.D. Klett, *Microphysics of Clouds and Precipitation*, pp. 177-180, D. Reidel, 1978.
- Sloan, J.J., Chemical and Physical Properties of Model Atmospheric Aerosols Measured by FTIR Extinction Spectroscopy, American Chemical Society meeting, Chicago, August 1995.
- Solomon, S., Progress towards a quantitative understanding of Antarctic ozone depletion, *Nature*, 347, 347-354, 1990.
- Tabazadeh, A., O.B. Toon, and P. Hamill, Freezing behavior of stratospheric sulfate aerosols inferred from trajectory studies, *Geophys. Res. Lett.* 22, 1725-1728, 1995.
- Tabazadeh, A., R.P. Turco, K. Drdla, and M.Z. Jacobson, A study of Type I polar stratospheric cloud formation, *Geophys. Res. Lett.*, 21, 1619-1622, 1994.
- Tolbert, M.A., Sulfate aerosols and polar stratospheric cloud formation, *Science*, 264, 527-528, 1994a.
- Tolbert, M.A., FTIR studies of low temperature sulfuric acid films and aerosols, Atmospheric Effects of Aviation Annual Meeting, Virginia Beach, 1994b.
- Toon, O.B., P. Hamill, R.P. Turco, and J. Pinto, Condensation of HNO₃ and HCl in the winter polar stratospheres, *Geophys. Res. Lett.*, 13, 1284-1287, 1986.
- Williams, L.R., and F.S. Long, Viscosity of supercooled sulfuric acid solutions, *J. Phys. Chem.*, 99, 3748-3751, 1995.
- Wuerker, R.F., H. Shelton, and R.V. Langmuir, Electrodynamic containment of charged particles, *J. Appl. Phys.*, 30, 342-349, 1959.
- Wyslouzil, B.W., K.L. Carleton, D.M. Sonnenfroh, W.T. Rawlins, and S. Arnold, Observation of hydration of single, modified carbon aerosols, *Geophys. Res. Lett.*, 21, 2107-2110, 1994.

Zeleznik, F.J., Thermodynamic properties of the aqueous sulfuric acid system to 350K, *J. Phys. Chem. Ref. Data*, 20, 1157-1200, 1991.

Zhang, R., P.J. Wooldridge, J.P.D. Abbatt, and M.J. Molina, Physical chemistry of the $\text{H}_2\text{SO}_4/\text{H}_2\text{O}$ binary system at low temperatures: Stratospheric implications, *J. Phys. Chem.*, 97, 7351-7358, 1993a.

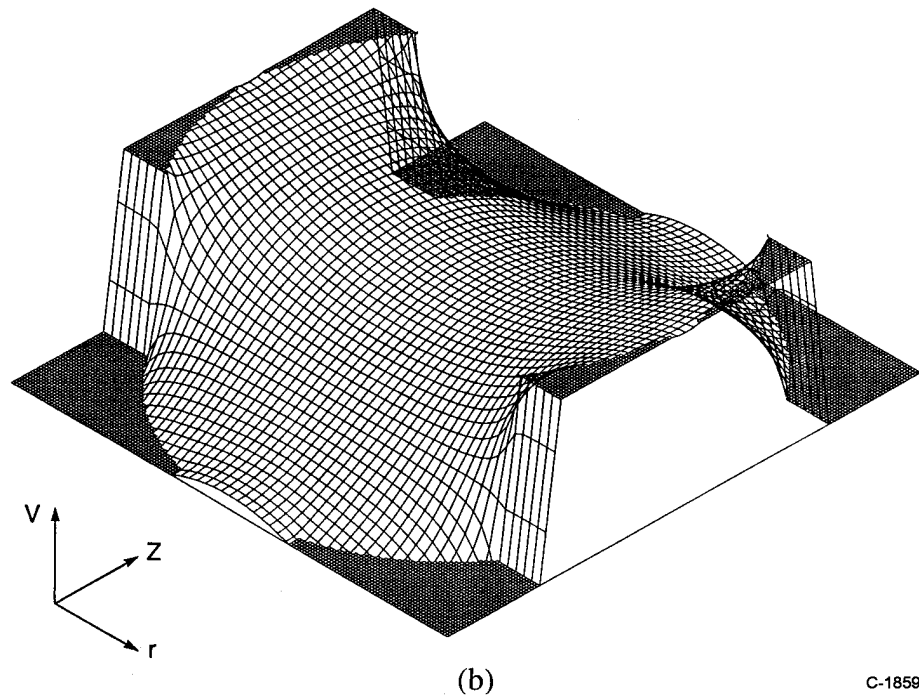
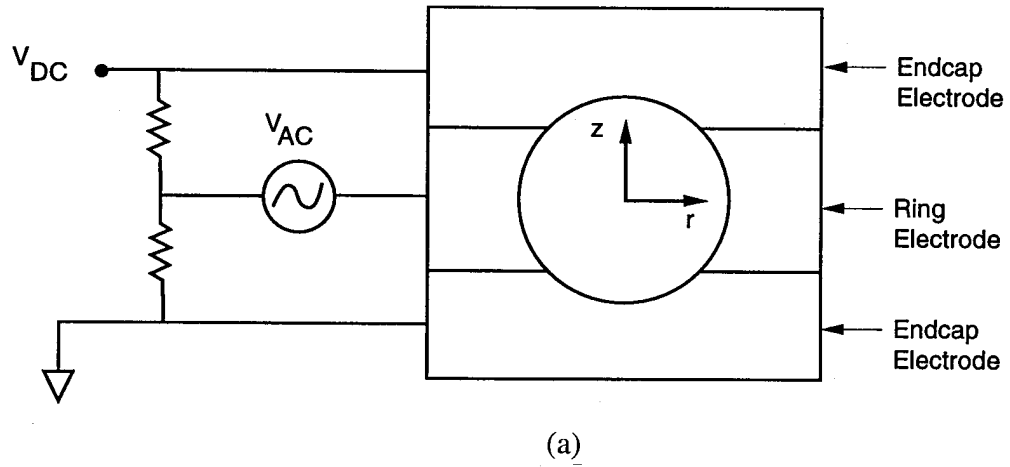
Zhang, R., P.J. Wooldridge, and M.J. Molina, Vapor pressure measurements for the $\text{H}_2\text{SO}_4/\text{HNO}_3/\text{H}_2\text{O}$ and $\text{H}_2\text{SO}_4/\text{HCl}/\text{H}_2\text{O}$ systems: Incorporation of stratospheric acids into background sulfate aerosols, *J. Phys. Chem.*, 97, 8541-8548, 1993b.

Table 1. Summary of endpoints for droplet freezing experiments

Composition (wt% H ₂ SO ₄)	Final Temperature °K	Degrees Supercooled °K	Equilibrium Phase	Final Phase
30.4	202.0	36.1	ice-liquid	solid
34.3	192	27.4	ice-SAH	liquid
37.7	191.8	22.6	SAH	liquid
46.6	192.6	37.7	SAT	liquid
59.7	195.2	48.7	SAT	liquid
60.7	191.4	51.9	SAT	liquid
64.1	199.4	38.0	SAT	liquid
70.9	199.2	33.0	SAD	liquid
77.2	198.8	59.9	SAM	liquid

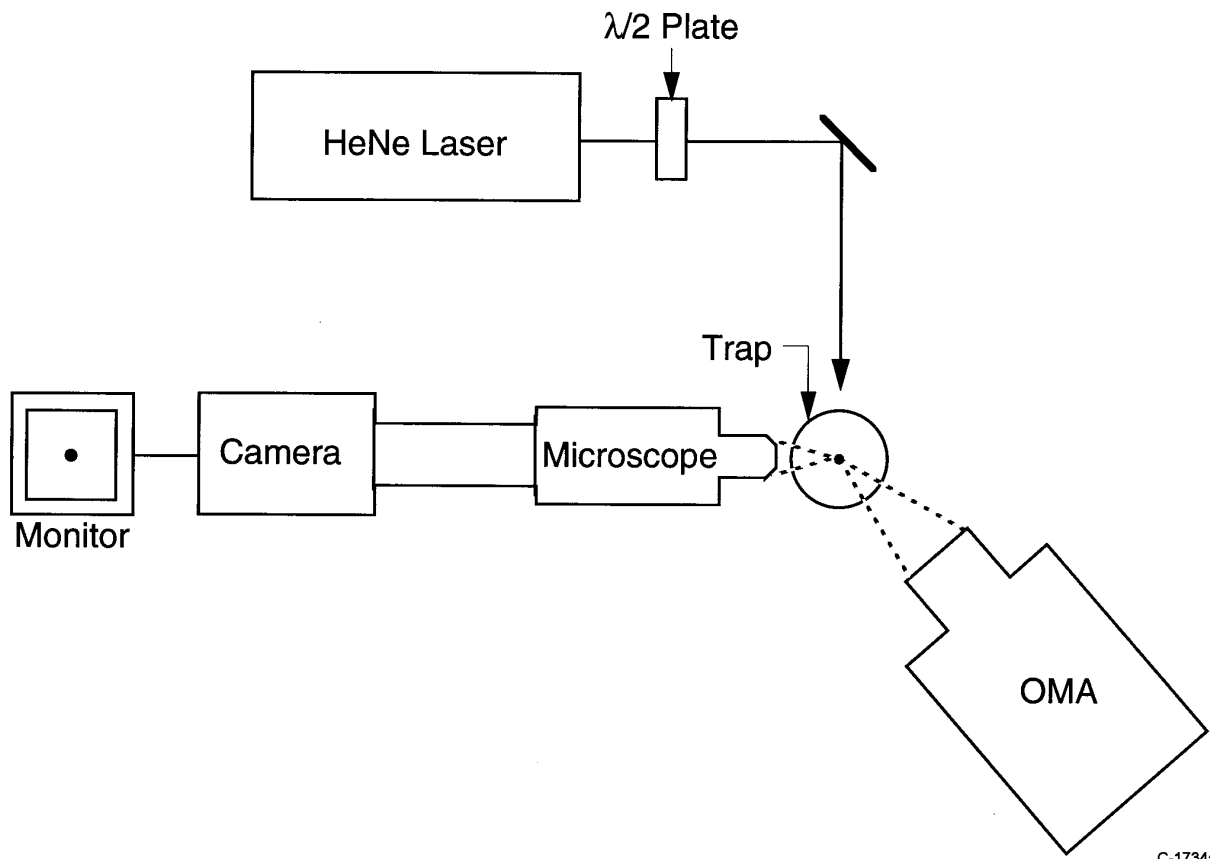
Table 2. Upper bound for the nucleation rate, J ($\text{cm}^{-3} \text{s}^{-1}$) based on drop volumes and observation times.

Composition (wt%)	Final Temperature °K	Final Drop Radius (μm)	Observation time (hr)	Upper bound J ($\text{cm}^{-3} \text{s}^{-1}$)
30.4	202.0	14.1	0.5	2430
34.3	192	15.4	0.75	1240
37.7	191.8	10.4	1	3020
46.6	192.6	12.6	1.25	1360
59.7	195.2	14.8	1	1050
60.7	191.4	12.4	3.25	549
64.1	199.4	15.4	3	310
70.9	199.2	11.5	0.13	17200
77.2	198.8	11.1	0.5	4970



C-1859

Figure 1. a) Spherical void electrodynamic levitator geometry and electronic circuitry and b) AC trapping potential computed for this geometry



C-1734a

Figure 2. Optical diagnostics including camera system for particle imaging and OMA for angularly resolved optical scattering.

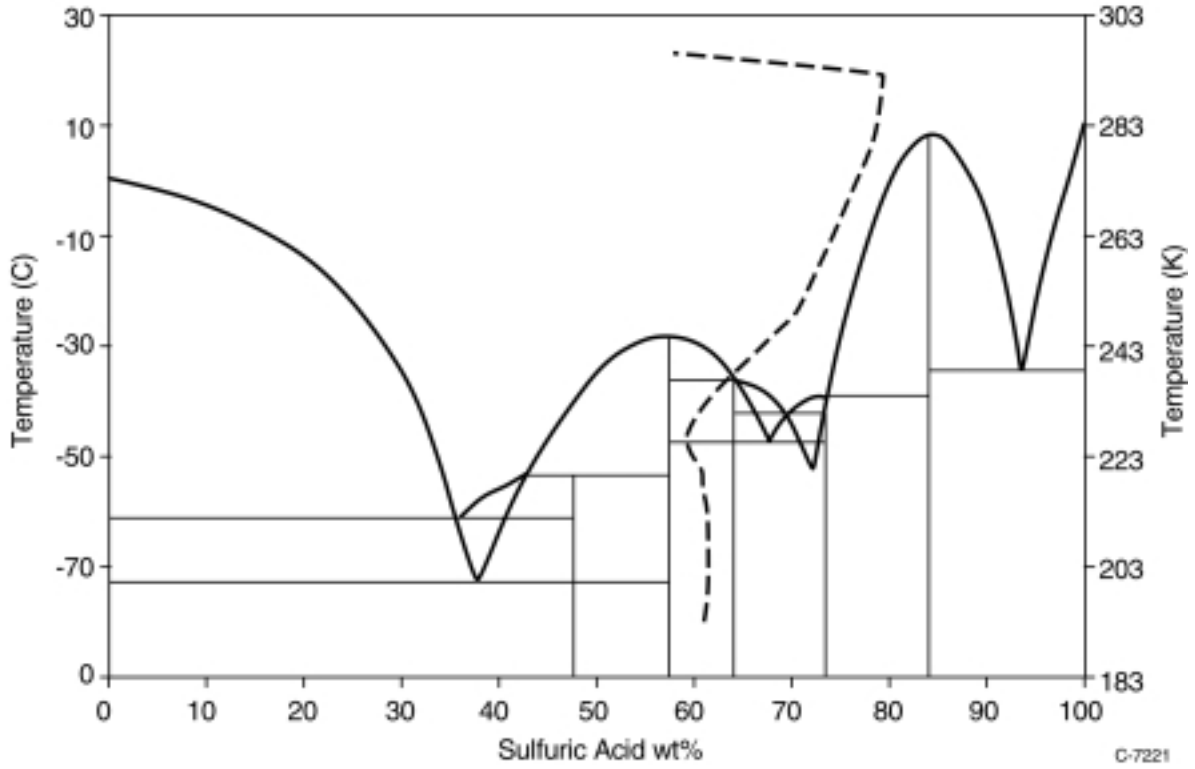
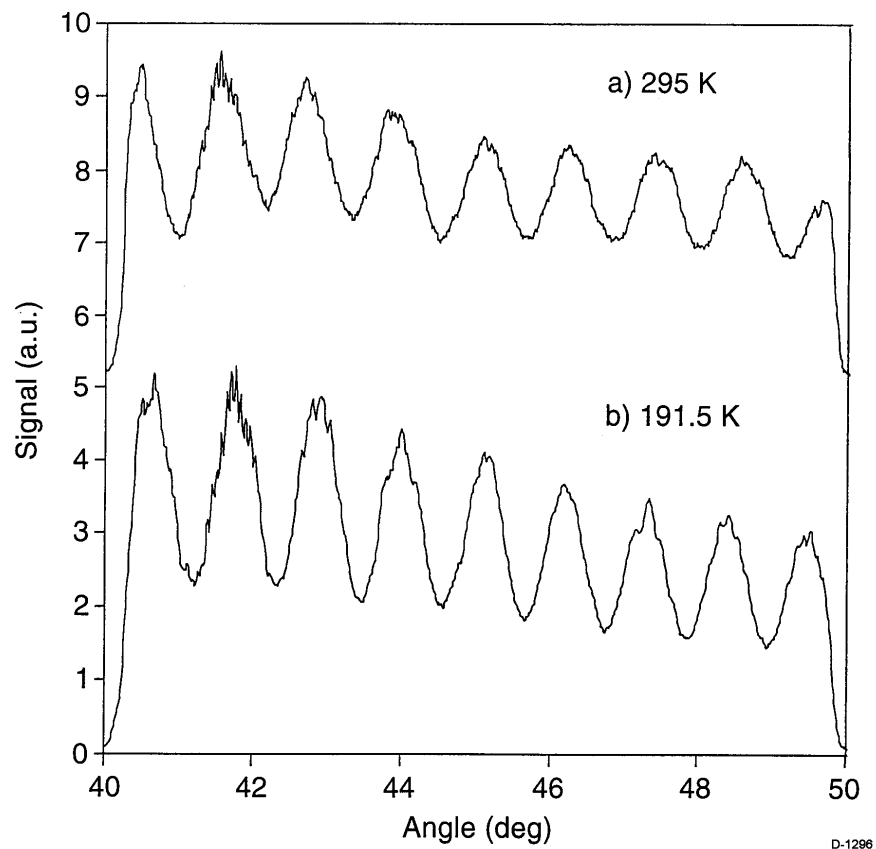


Figure 3. Trajectory for cooling single sulfuric acid droplet superimposed on H₂SO₄/H₂O phase diagram of *Gable et al.*, [1950]. The tie lines define two-phase equilibrium boundaries.



D-1296

Figure 4. Angularly resolved Mie scattering pattern for sulfuric acid droplet: a) 295 K, 50 wt% and b) 191.5 K, 61 wt%.

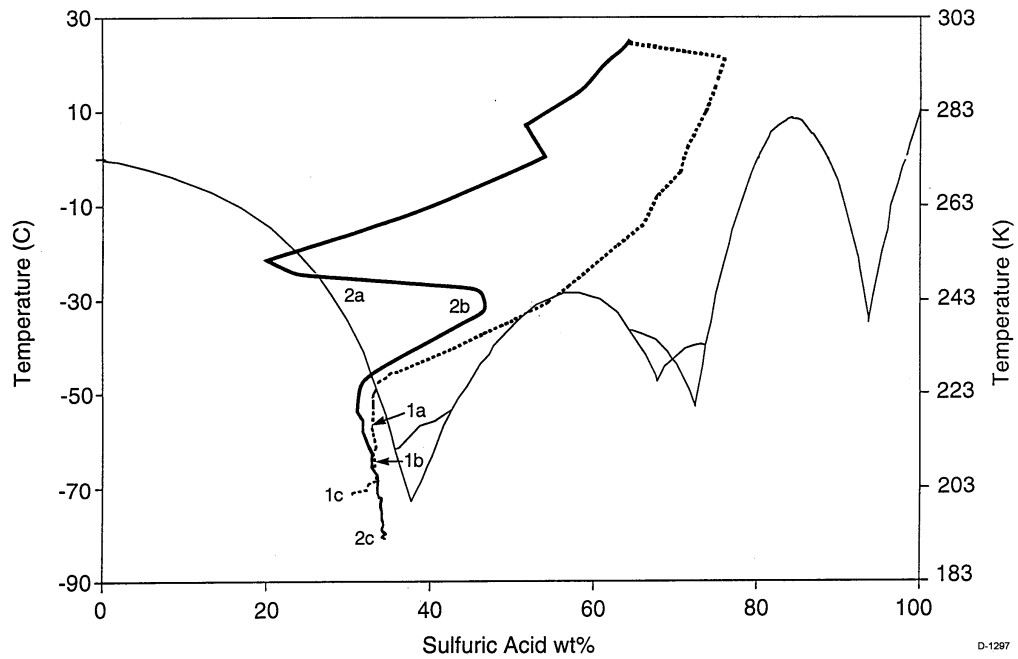


Figure 5. Two different trajectories of particle composition during cooling through the ice-liquid equilibrium region.

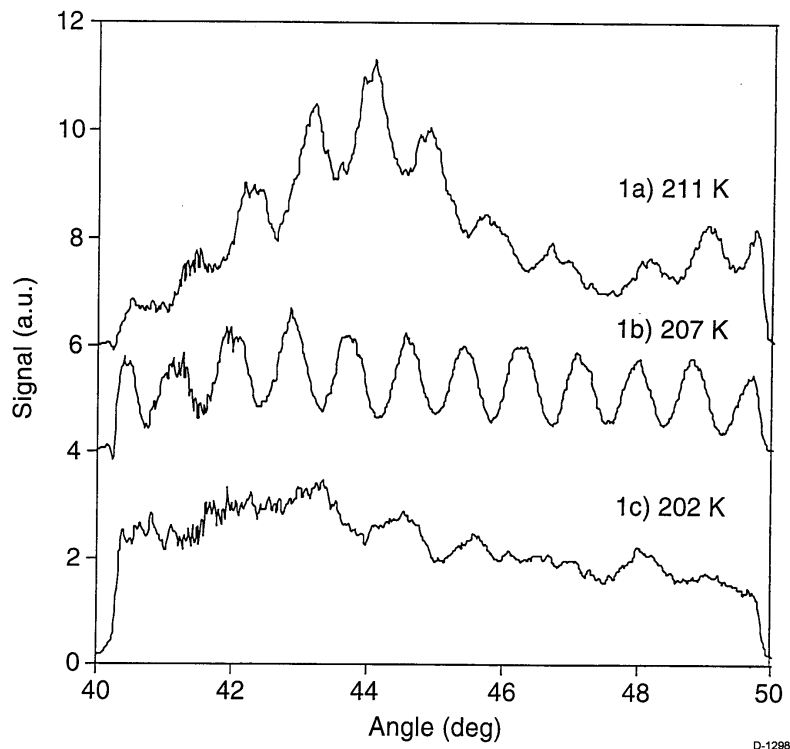


Figure 6. Angular scattering patterns for particle trajectory #1 shown in Figure 5.

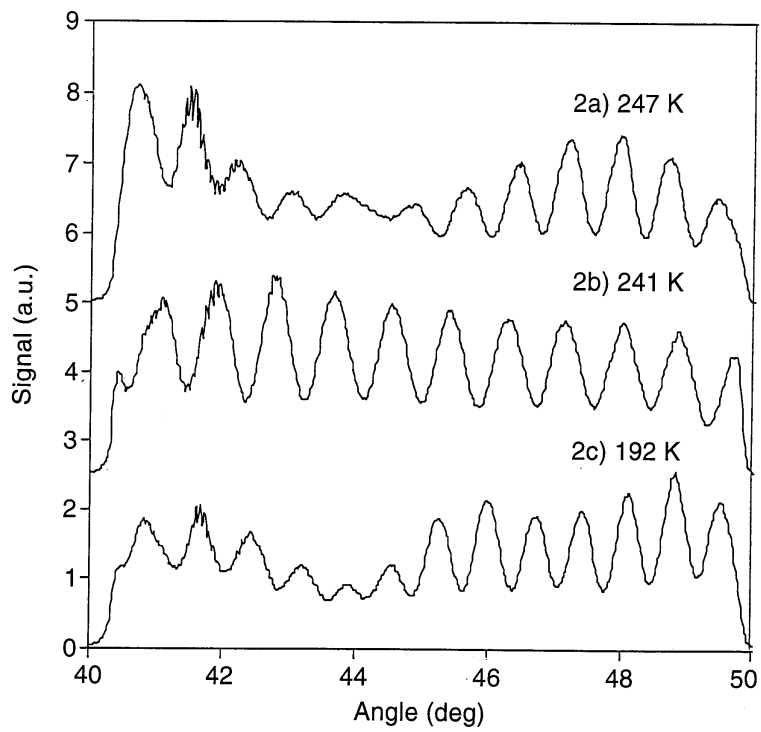


Figure 7. Angular scattering patterns for particle trajectory #2 shown in Figure 5.

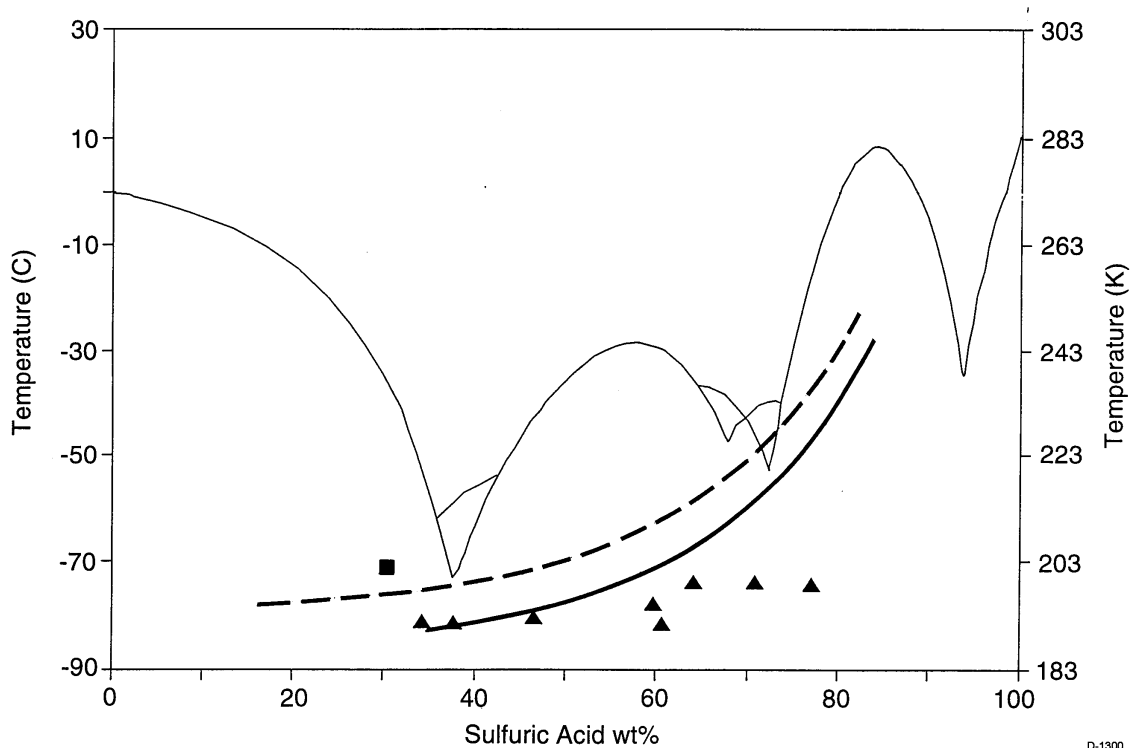


Figure 8. Summary of endpoints for sulfuric acid droplet cooling experiments plotted on H₂SO₄/H₂O phase diagram. Curves are equilibrium sulfuric acid compositions for fixed water partial pressures of 1×10^{-4} (solid curve) and 4×10^{-4} torr (dashed curve).